Synthesis, Characterization, and Rietveld Refinement of Tungsten-Framework-Doped Porous Manganese Oxide (K-OMS-2) Material

Craig Calvert, Raymond Joesten, Katana Ngala, Josanlet Villegas, Aimee Morey, Xiongfei Shen, and Steven L. Suib*

Department of Chemistry, Unit 3060, 55 North Eagleville Road, University of Connecticut, Storrs, Connecticut 06269-3060

Received April 28, 2008. Revised Manuscript Received August 9, 2008

Tungsten was successfully doped at 1 and 2 mol % tungsten into the K-OMS-2 framework. Sodium tungstate and tungsten pentabromide were used in a reflux synthesis preparation. The data collected from the characterization methods collectively affirm the substitution of tungsten into the K-OMS-2 framework. Conductivity measurements showed an increase in the resistivity. Conversion of benzyl alcohol to benzaldehyde had a conversion of 25 and 15% for the sodium tungstate and tungsten pentabromide, respectively, while retaining 100% selectivity. Properties such as the resistivity, thermal stability, and crystallinity of the material were altered depending on the amount and type of starting reactants used.

Introduction

This paper concerns the doping of tungsten into the framework of K-OMS-2 (cryptomelane). K-OMS-2 has been doped with Mg,[1] Al,[1] V,[2] Cr,[3] Fe,[4−6] Co,[1,5,7] Ni,[1,5] Cu,[1,4,5,7] Zn,[1,5] and Ag.[7] Crystal radius considerations suggest that these cations, with the exception of Ag, enter the octahedral framework, replacing Mn. Note that $^{VIII}K^{1+}$ in the tunnel site is readily exchanged with H^{1+}, Rb^{1+}, Cs^{1+}, and Ba^{2+}.[8] A novel exchange mechanism involving octahedral vacancies is proposed to satisfy the charge imbalance that results from introduction of hexavalent W into the α-MnO_2 structure. In the 1950s, one of the first synthetic procedures for K-OMS-2 was reported.[9] The synthesis of this material was driven by the need for pure phase and highly crystalline materials, as the natural minerals were not pure phases and contain a wide range of compositions. Such materials have been used in catalysis,[10] battery materials,[11] and molecular sieve applications.[12] This has led to increased interest in the analysis and synthesis of these materials.

The structures of α-$MnO_2$and K-OMS-2 consists of double-wide slabs of edge-shared MnO_6^{8-} octahedra, aligned approximately parallel to (110), to form tunnels with a square cross-section. The tunnels are bounded by four $Mn_2O_6^{4-}$ slabs, each rotated 90° to its neighbor, and joined through corner-shared oxygens. The VIII-coordinated tunnel site may be vacant or occupied by H_2O or large cations.

K-OMS-2 is mixed valent α-MnO_2 in which charge imbalance on the octahedral framework due to reduction of Mn^{4+} to Mn^{3+} is compensated by $^{VIII}K^{1+}$ in the tunnel site. This exchange, called the redox exchange by Feng et al.[13] gives the general formula, $K_XMn^{4+}{}_{1-X}Mn^{3+}{}_XO_2$

$$^{VI}Mn^{3+} + {}^{VIII}K^{1+} \rightarrow {}^{VI}Mn^{4+} + {}^{VIII}\square^{\circ} \quad (1)$$

where ($^{VIII}\square^{o}$) is a vacant tunnel site.

The unit cell (*I*4/*m*) contains 16 oxygen sites, 8 six-coordinated Mn sites, and 2 eight-coordinated tunnel sites. Because the crystal radius of $^{VIII}K^{1+}$ (1.65Å, C.R. data set in Shannon[14,15]) is greater than 1/2 the c-translation of K-OMS-2, fractional occupancy of the tunnel site is typically 0.5, resulting in $X = 0.125$ and a formula of $K_{0.125}Mn^{4+}{}_{0.875}Mn^{3+}{}_{0.125}O_2$, with an average oxidation state, AOS = 3.875. We will use this formula, in which the number of $^{VI}Mn^{3+}$ is equal to the number of $^{VIII}K^{1+}$, with a maximum of 0.125 $^{VIII}K^{1+}$ per formula as the basis for evaluation of exchanges for introduction of $^{VI}W^{6+}$ into the octahedral framework of K-OMS-2. Because the crystal radius of $^{VI}W^{6+}$ (0.74 Å) lies between those of $^{VI}Mn^{3+}$ low spin (LS) (0.72 Å) and $^{VI}Mn^{3+}$ high spin (HS) (0.785 Å) and is somewhat larger than that of $^{VI}Mn^{4+}$ (0.67Å), it is

* Corresponding author. Phone (860) 486-2797. Fax: (860) 486-2981. E-mail: steven.suib@uconn.edu.

(1) Chen, X.; Shen, Y. F.; Suib, S. L.; O'Young, C. L. *Chem. Mater.* **2002**, *14*, 940.
(2) Polverejan, M.; Villegas, J. C.; Suib, S. L. *J. Am. Chem. Soc.* **2004**, *126*, 7774.
(3) Ching, S.; Driscoll, P.; Kieltyka, K.; Marvel, M.; Suib, S. *J. Chem. Soc., Chem. Commun.* **2001**, *23*, 2486.
(4) DeGuzman, R.; Shen, Y.; Neth, E.; Suib, S.; O'Young, C.; Levine, S.; Newsam, J. *Chem. Mater.* **1994**, *6*, 815.
(5) Zhou, H.; Wang, J. Y.; Chen, X.; O'Young, C. L.; Suib, S. L. *Microporous Mesoporous Mater.* **1998**, *21*, 315.
(6) Cai, J.; Liu, J.; Willis, W. S.; Suib, S. L. *Chem. Mater.* **2001**, *13*, 2413.
(7) Xia, G. G.; Yin, Y. G.; Willis, W. S.; Wang, J. Y.; Suib, S. L. *J. Catal.* **1999**, *185*, 91.
(8) Post, J. E.; Bish, D. L. *Rev Mineral.* **1989**, *20*, 277.
(9) De Carvalho, A. *J. Appl. Chem.* **1957**, *7*, 145.
(10) Duan, N.; Suib, S.; O'Young, C. *J. Chem. Soc., Chem. Commun.* **1995**, *13*, 1367.
(11) Shen, Y.; Suib, S.; O'Young, C. *J. Am. Chem. Soc.* **1994**, *116*, 11020.
(12) Wasserman, S.; Carrado, K.; Yuchs, S.; Shen, Y.; Cao, H.; Suib, S. *Physica B.* **1995**, *208 & 209*, 674.
(13) Feng, Q.; Kanoh, H.; Miyai, Y.; Ooi, K. *Chem. Mater.* **1995**, *7*, 148.
(14) Shannon, R. D.; Prewitt, C. T. *Acta Crystallogr., Sect. B* **1969**, *25*, 925.
(15) Shannon, R. D. *Acta Crystallogr., Sect. A* **1976**, *32*, 751.

10.1021/cm801146m CCC: $40.75
Published on Web 09/25/2008

hypothesized that W substitutes for Mn in the octahedral framework of K-OMS-2.

In this paper, selected synthesis and characterization methods were utilized to test the location of the tungsten doped into the K-OMS-2 material. Tungsten pentachloride and sodium tungstate precursors were used as the doping compounds to test the effects of a bromide precursor and water-soluble oxide precursor on the structures and reactivity of the doped material. Once synthesized, the presence of discoloration of the typically dark brown K-OMS-2 might indicate the formation of tungsten oxides such as WO_3 (yellow). Tungsten and manganese have different crystal radii, and if tungsten is doped into the K-OMS-2 crystal structure, then possible changes could occur in the morphology due to the differences in the crystal radii. Such changes in morphology can be examined using scanning electron microscopy (SEM) analysis. Elemental analysis was done concurrently with SEM analysis and provided qualitative elemental analysis. The crystal formula calculated from the energy-dispersive spectroscopy (EDS) data can be used to provide relationships between composition and the structural and chemical data. The insertion of a tungsten cation into the material could change the ratio of Mn^{3+} to Mn^{4+} and be indicated by a change in the average oxidation state of manganese of the material. Structural data from powder X-ray diffraction is key, because disruption of the structure of K-OMS-2 would cause the loss of important physical properties, such as porosity, that attribute to the chemical properties of K-OMS-2. Tungsten forms numerous oxides with octahedral building blocks,[16−18] so if a tungsten octahedra of the appropriate size can be formed around the tungsten atom, then tungsten could be doped into the K-OMS-2 framework. Previous work on framework doping has shown an upper limit in dopant that can be integrated into the framework before impurities are formed;[19] in this work, the effect of dopant amount on the structure will be analyzed with powder X-ray diffraction (XRD). Refinement of the XRD patterns will produce a structural model that will provide valuable insight into the location of the tungsten dopant. If tungsten is doped into the material then the refractory nature of tungsten might produce a more thermally stable material with a higher resistivity than undoped K-OMS-2. The inclusion of tungsten, which is more massive than manganese, may affect the atom-to-atom vibrational interactions that can be studied with Raman spectroscopy. Such insertion in the framework can generate different vibrational modes than the pure material from added tungsten to oxygen bonds. The combination of these analytic methods with some intrinsic properties of tungsten were utilized to disclose the location of tungsten in the K-OMS-2 framework.

The Rietveld method is a powerful tool for crystal structure refinement of materials that are too fine-grained for single-crystal XRD determination, like the synthetic K-OMS-2 presented here. Rietveld refinement involves the iterative least-squares fitting of the XRD powder pattern calculated for a starting structure with that measured on the sample material. Post et al. determined the structure of the natural monoclinic (*I* 2/*m*) analogue of K-OMS-2, cryptomelane, by single-crystal methods[20] and demonstrated that Rietveld refinement of the same material[8] yielded lattice parameters and atom coordinates with comparable accuracy and precision. Although Rietveld refinement of synthetic α-MnO_2[21,22] and K-OMS-2[4,23] are reported, there are no refinements of doped K-OMS-2 materials.

Methods

Synthesis. A potassium permanganate solution was prepared by adding 50 mL of distilled water to a beaker containing mixed dry potassium permanganate, Across, ACS reagent 99+%, dopant (tungsten pentabromide, Aldrich, or sodium tungstate dihydrate, Mallinckrodt analytic reagent), if used. The mass of the permanganate to dopant was determined by the desired mole ratio of manganese to tungsten. The amount of permanganate was kept close to 5 g to ensure similar mass transfer with the established reflux method. A manganese sulfate solution was prepared by mixing manganese sulfate, Sigma Aldrich 98+%; water, 33 mL; and nitric acid, 6.8 mL, JT Baker 66−70%. The amount of manganese sulfate was again varied depending on the desired ratio of tungsten to manganese. The manganese sulfate solution was added dropwise over 15 min to a stirred solution of the potassium permanganate solution. After being mixed, the resulting solution was refluxed overnight at 100 °C, washed and filtered, and then dried at 100 °C overnight. The yield for the synthesis was between 40 and 70% or 4 and 6 g with between 5 and 9 total grams of manganese reactant.

Nomenclature. When referring to the mole ratios of tungsten to manganese, a 1% sample means 1 mol of tungsten to 100 mol of manganese. When tungsten pentabromide was used in the synthesis, the material is labeled as WBr following the ratio ex. 1% WBr. When sodium tungstate was used in the synthesis, the material is labeled as W-ate following the ratio ex. 1% W-ate. The mole percents are those from the theoretical mole ratios from the synthesis, not from the sample analysis.

Characterization

Powder X-ray Diffraction (XRD). Synthesized material was ground in an agate mortar and front-loaded into a Pb sample holder by pouring powder into the well and scraping off excess with a straight edge. Digital XRD spectra were acquired with a Scintag model PDS-2000 using Cu Kα at 45 kV and 40 ma, with a continuous scan from 5 to 65° 2θ, at 1° 2θ/min. Diffraction peaks for Pb, (111) at 31.30° and (002) at 36.0°, marked with a "*" in Figures 1 and 2, served as an internal standard. Diffraction peaks were indexed using JCPDS file 29−1020, synthetic KMn_8O_{16}, space group (*I*4/*m*).

Scanning Electron Microscopy (SEM)/Energy-Dispersive X-ray Analysis (EDS). The ground sample from the XRD analysis was sprinkled onto carbon tape on an SEM stub. Imaging and EDS analysis were performed with an Amray model 1810 D operated at 20 kV with X-ray spectra acquired and processed with an Amray

(16) Cotton, F.; Wilkinson, G. *Advanced Inorganic Chemistry*, 4th ed.; Wiley-Interscience: New York, 1980.
(17) Tilley, R. *Int. J. Refract. Met. Hard Mater.* **1995**, *13*, 93.
(18) Gerand, B.; Seguin, L. *Solid State Ionics* **1996**, *84*, 199.
(19) Cai, J.; Suib, S. *Inorg. Chem. Commun.* **2001**, *4*, 493.
(20) Post, J. E.; Von Dreele, R. B.; Buseck, P. R. *Acta Crystallogr.* **1982**, *B38*, 1056.
(21) Rossouw, M. H.; Liles, D. C.; Thackeray, M. M.; David, W. I. F.; Hull, S. *Mater. Res. Bull.* **1992**, *27*, 221230..
(22) Kijima, N.; Ikeda, T.; Oikawa, K.; Izumi, F.; Yoshimura, Y. *J. Solid State Chem.* **2004**, *177*, 1258.
(23) Xiao, T.; Bokhimi, F.; Benaissa, M.; Perez, R.; Strutt, P. R.; Yacaman, M. J. *Acta Met. Mater.* **1997**, *45*, 1685.

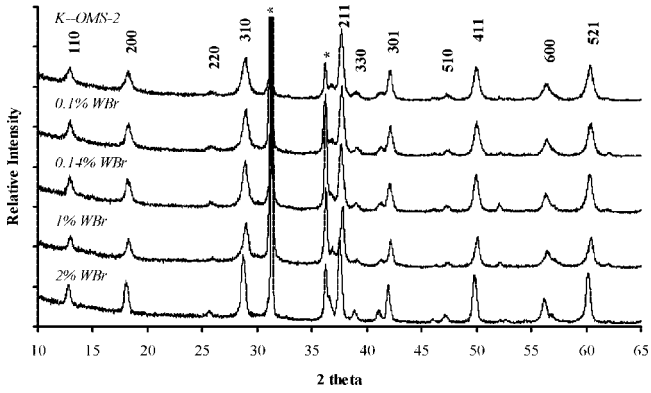

Figure 1. Powder X-ray diffraction patterns of the WBr samples from 0.1 to 2% doping with a reference K-OMS-2 pattern and an * designating the lead sample holder peaks. The peaks were indexed according to the JCPDS file 29−1020.

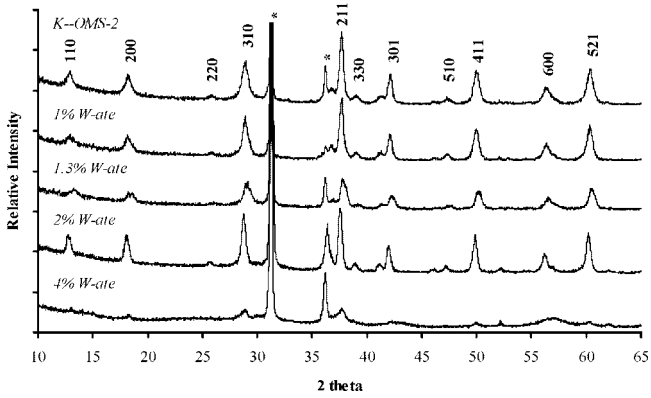

Figure 2. Powder X-ray diffraction patterns of the W-ate samples from 1 to 4% doping with a reference K-OMS-2 pattern and an * designating the lead sample holder peaks. The peaks were indexed according to the JCPDS file 29−1020.

model PV 9800 EDS system. Elemental k-values for K K_α, Mn K_α, and W L_α were calculated relative to pure elements by the standardless method. Element concentrations, reported as weight percent metal in Table 1, were calculated by the ZAF method. Effect of oxygen on X-ray intensity was not included in the matrix calculation. Each sample was sampled at a minimum of seven spots and the numbers were averaged. Some samples were analyzed as many as three times to check reproducibility.

Thermogravimetric Analysis (TGA). TGA was carried out with a Perkin-Elmer TGA 7 Thermogravimetric Analyzer with Pyrex software. Before analysis, samples were dried in a desiccator to remove absorbed water. The temperature range was set from room temperature (about 23 °C) to 800 °C and increased at 5 °C/min. The runs were performed in a nitrogen atmosphere. The data were plotted from 50 to 800 °C.

Raman. Raman spectroscopy was done with a Renishaw Ramanscope at 514 nm with Wire 2.0 Software. Spectra were collected at 64 scans with a scan rate of 126 per minute. Each sample was sampled at a minimum of five spots, and some samples were analyzed as many as three times to check reproducibility.

Average Oxidation State (AOS). The average oxidation state of manganese was obtained by a potentiometric titration method.[24] First, the material was reduced to Mn^{2+} using concentrated HCl and titrated to Mn^{3+} using a $KMnO_4$ standard solution to obtain the total amount of manganese. Next, the AOS of manganese was determined by reducing to Mn^{2+} with $(NH_3)_2Fe(SO_4)_2$ and back-titrating the excess Fe^{2+} with the $KMnO_4$ standard solution.

Resistivity. Samples were pressed into approximately 1 mm thick disks with a diameter of 13.1 mm. The pellets were pressed for one minute at 10 000 lbs/in^2. The samples were secured to standard glass microscope slides with a nonconducting epoxy resin. Silver wires were then attached to the disks with a conductive silver paint. DC resistivities of the W substituted K-OMS-2 materials were measured at room temperature by the four-probe method.[24]

Oxidation Reaction. The oxidation capability was investigated using the oxidation of benzyl alcohol to benzaldehyde. The reaction of K-OMS-2 with a 100% conversion and 100% selectivity was used as a reference and is detailed in previous work.[25]

Rietveld Refinement. Structures of two W-doped samples, 1.33% W-ate and 2% W-ate, and a reference K-OMS-2 were refined by Rietveld analysis of XRD spectra of ground powders, back-loaded into an Al sample holder without packing, and step scanned at 0.02° 2θ per step, 10s counting time, with the Scintag XDS2000, using Cu Kα at 45 kV and 40 mA. The starting structure for refinement using GSAS40 is that of synthetic α-MnO_2.[21] Fractional coordinates of K (0, 0, 0.5) and the site occupancy of oxygens O_1 and O_2 were held fixed in the refinement.

Results

Synthesis. The synthesis of the doped material was a straightforward procedure, except tungsten pentabromide slowly oxidizes in air. This led to inconsistent results when using samples from opened jars. Oxidation was indicated by color changes in the tungsten pentabromide after exposure to the atmosphere, so small 5 g jars were purchased and used within a week of opening with nitrogen purging between uses. The tungsten pentabromide samples evolved a dark brownish red gas, Br_2, after about 10 min of heating. After reacting overnight, there was no evidence of any dark gas in the condenser. The sodium tungstate did not form this dark gas. The observed bromine gas was due to the hydrolysis of tungsten pentabromide to tungstic acid. No yellow color or particles were observed from tungsten trioxide in the synthesized material.

Powder X-ray Diffraction. XRD patterns for [W] K-OMS-2 synthesized using WBr_5 and Na_2WO_3 are shown in Figures 1 and 2, with an XRD pattern of pure K-OMS-2 synthesized by the reflux method, for reference. The XRD patterns shown in Figure 1 and 2 were obtained using relatively short scan times and are intended for the identification of primary features in the pattern. A more meticulous preparation procedure and instrument scan must be used to generate more precise patterns for Reitveld analysis, accurate determination of peak shifting, and other more nuanced features. Diffraction peaks are labeled with indices for synthetic tetragonal ($I4/m$) KMn_8O_{16}, JCPDS file 29−1020. Diffraction patterns are essentially identical for W-doped (excluding the 4% W-ate) and reference K-OMS-2 and there is no systematic variation of peak location, peak shape, or peak intensity, with composition. Compared with JCPDS file 29−1020, the intensity of the (220) reflection is suppressed, and intensities of peaks with $2\theta > 40°$ are enhanced. No additional peaks due to tungsten metal, tungsten oxides, or other impurities were identified.

(24) Glover, D.; Schumm, B., Jr.; Kozowa, A. *Handbook of Manganese Dioxides Battery Grade*; International Battery Materials Association: Cleveland, OH, 1989.
(25) Makwana, V.; Garces, J.; Liu, J.; Cai, J.; Son, Y.; Suib, S. *Catal. Today* **2003**, *85*, 225.

Table 1. Elemental, Conductivity, and Oxidation Properties of Synthesized K-OMS-2 and [W] K-OMS-2 Materials

wt %	K-OMS-2	0.14%WBr	1% W-ate	1% WBr	2% W-ate	2% WBr
			Energy-Dispersive X-Ray Analysis (EDS)			
K	5.7	5.4	6.0	5.8	6.0	5.6
Mn	94.3	94.3	90.3	90.9	88.1	87.6
W	0	0.3	3.7	3.4	5.9	6.9
total	100	100	100	100	100	100
			Formula Proportion Based on $K_XW_Y\square^\circ_Y Mn^{4+}{}_{1-X}Mn^{3+}{}_{X-2Y}O_2$, Normalized to $n_{Mn} + 2n_W = 1$			
mol of K	0.085	0.080	0.092	0.087	0.092	0.085
mol of Mn total	1	0.998	0.976	0.978	0.961	0.955
mol of Mn3+	0.085	0.078	0.068	0.066	0.054	0.040
mol of Mn4+	0.915	0.920	0.908	0.913	0.908	0.915
mol of W	0	0.001	0.012	0.011	0.019	0.022
Σ VI-fold cations	0.999	0.988	0.989	0.981	0.978	
mol of oxygen	2	2	2	2	2	2
AOS calcd	3.92	3.92	3.93	3.93	3.94	3.96
AOS measd	3.88	ND[a]	ND[a]	3.86	ND[a]	3.95
resistivity ρ (Ω cm)	$4.4 \times 10^{2(4)}$	2.9×10^2	ND[a]	ND[a]	$>5 \times 10^4$	$>5 \times 10^4$
			Oxidation of Benzyl Alcohol to Benzaldehyde			
% conversion	100[25]	ND[a]	25	15	27	15
% selectivity	100[25]	ND[a]	100	100	100	100

[a] ND = no data taken.

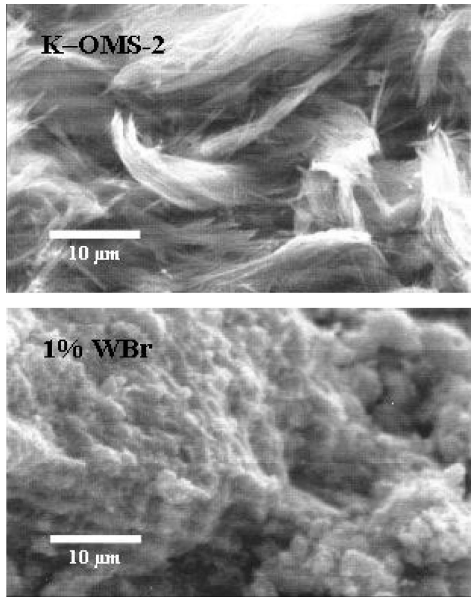

Figure 3. SEM micrographs of K-OMS-2 samples. The top image is of the K-OMS-2 reference sample showing a long fibrous morphology. The bottom image is the 1% WBr sample showing a less fibrous morphology than the standard K-OMS-2 and is representative of the tungsten-doped K-OMS-2 samples.

The XRD data demonstrate that [W] K-OMS-2 was successfully synthesized from starting mixtures with 0.1, 0.14, 1, and 2 mol% WBr_5 and 1, 1.3, and 2 mol% $Na_2WO_3 \cdot 2H_2O$. All attempts to synthesize [W] K-OMS-2 with a concentration of 4 mol% or more tungsten, failed to produce a significant amount of crystalline K-OMS-2. An XRD pattern for one example, 4% W-ate (Figure 2), is dominated by the (111) and (002) peaks for the Pb internal standard, but shows very small peaks corresponding to (110), (200), (310), (211), (411), and (521) reflections for K-OMS-2. Separating the crystalline material from amorphous material in the sample for further characterization was not possible.

Scanning Electron Microscopy. K-OMS-2 has a fibrous morphology as shown in a representative image in Figure 3. SEM images of the W doped samples showed that globular particles were produced-as shown in a representative image in Figure 3. In addition, micrographs (not shown) showed similar morphologies independent of precursor or dopant amount.

Energy-Dispersive X-Ray Spectroscopy/AOS. Elemental EDS analyses of K-OMS-2 and [W] K-OMS-2 are reported in Table 1. The values are reported as weight% metal, and a formula was derived based on the proposed model for substitution of a $^{VI}W^{6+}$ atom and a vacancy ($^{VI}\square^\circ$) for two octahedrally coordinated Mn^{3+} atoms in K-OMS-2, $K_XW_Y\square^\circ_Y Mn^{4+}{}_{1-X}Mn^{3+}{}_{X-2Y}O_2$. Molar proportions of Mn^{4+} and Mn^{3+} in the formulas ($n_{Mn^{4+}}$ and $n_{Mn^{3+}}$), and the calculated average oxidation state (AOS) are given by $n_{Mn^{3+}} = n_{Mn} - (n_K + 2n_W)$ and $n_{Mn^{4+}} = n_{Mn} - n_{Mn^{3+}}$. The EDS results are semiquantitative because the EDS spectra were acquired from rough-surfaced, as-grown aggregates. K-values were computed by the standardless method, and the ZAF correction procedure did not include the effect of oxygen on X-ray intensity. Analyses of reflux-grown K-OMS-2 fit the K-OMS-2 formula, $K_XMn^{4+}{}_{1-X}Mn^{3+}{}_XO_2$, and match closely the values obtained by atomic absorption analysis of sol gel synthesized material grown in our laboratory,[26] 7.6% K, 92.4% Mn, and AOS = 3.87,[27] with the formula, $K_{0.115}Mn^{4+}{}_{0.87}Mn^{3+}{}_{0.13}O_{1.99}$. This surprisingly close fit to the K-OMS-2 formula is probably the result of the fact that these materials are nearly pure MnO_2, so that the impact of potentially large errors in the measurement of small concentrations of K and W is minimal. For given %W in the starting mixture, the composition of [W] K-OMS-2 produced by the two synthesis formulations are essentially identical. Formulas for 1% W and 2% W (Table 1) are

$$K_{0.09}W^{6+}{}_{0.01}\square^\circ{}_{0.01}Mn^{4+}{}_{0.91}Mn^{3+}{}_{0.07}O_2, \quad AOS_{calcd} = 3.93,\ AOS_{obsd} = 3.86 \quad (2)$$

and

(26) Ching, S.; Petrovay, D. J.; Jorgensen, M. L.; Suib, S. L. *Inorg. Chem.* **1997**, *36*, 883.
(27) Ching, S.; Roark, J. L.; Duan, N.; Suib, S. L. *Chem. Mater.* **1997**, *9*, 750.

$$K_{0.09}W^{6+}_{0.02}\square^{\circ}_{0.02}Mn^{4+}_{0.91}Mn^{3+}_{0.05}O_2,$$
$$AOS_{calcd} = 3.95,\ AOS_{obsd} = 3.95 \quad (3)$$

The AOS for the reference K-OMS-2 value was 3.88, indicating an increase in the AOS as more tungsten is added.

Thermogravimetric Analysis. The TGA data of the 1 and 2% W-ate and WBr samples are shown in Figure 4 along with a the reference undoped K-OMS-2. Compared to K-OMS-2 the weight loss of the doped samples, as evidenced by the slope, occurred faster and at lower temperatures.

The W-ate temperature profiles both had the initial weight losses at 425 °C and the second weight loss at 600 °C, and the slope of the 2% doped material was larger and subsequently caused more overall weight loss. The final weight percent for the 1% W-ate sample was 91.7%, whereas the 2% W-ate sample was 90.5%. The WBr temperature profiles had the initial weight loss at 440 °C and the second weight loss at 575 °C and showed variance in the slope of the temperature profile. The 1% WBr doped material had a similar slope as the W-ate samples up to 650 °C, but the slope above 650 °C was larger and subsequently caused more overall weight loss. The 2% WBr doped material showed a larger slope than the other samples starting at 450 °C. Both WBr samples had a final weight percent of 88.2%. The TGA temperature profiles showed that undoped K-OMS-2 was more thermally stable than doped K-OMS-2. However, samples doped with tungstate and samples with lower tungsten doping were more thermally stable.

Raman. The Raman data, Figure 5, shows a representative spectrum of the synthesized samples. This spectrum shows two characteristic peaks of K-OMS-2 around 580 and 650 cm^{-1}. The strong peak at 650 cm^{-1} corresponds to the A_{1g} vibrational mode and the weaker shoulder peak corresponds to the F_{2g} vibrational mode.[28] These peaks are attributed to the Mn−O lattice vibrations of the [MnO_6] octahedron.[29] The relative intensities of these peaks are also in agreement with K-OMS-2.[30] The major peaks of WO_3 at 710 and 800 cm^{-1},[31] WO_4^{2+} compounds at 909 cm^{-1},[32] and WO_2 at 790 and 881 cm^{-1}[32] were not observed.

Resistivity. The resistivity measurements are shown in Table 1. A sample with the ratio of 0.14% showed a resistivity value of 3×10^2 Ω cm, which is similar to K-OMS-2, 4×10^2 Ω cm. The resistivity values for the other samples tested were not in the range of this experimental method due to the high resistivity of the material, $>5 \times 10^4$ Ω cm. The resistivity values were at least 2 orders of magnitude greater than K-OMS-2.

Oxidation Reaction. The doped materials converted benzyl alcohol to benzaldehyde, Table 1. The sodium tungstate precursor had conversions of 25 and 27 mol % at values of 1 and 2%, respectively, while maintaining 100% selectivity toward benzaldehyde. The tungsten pentabromide at both 1% and 2% mole ratio showed conversions of 15%, while also maintaining 100% selectivity toward benzaldehyde. When compared to K-OMS-2 the doped materials had lower conversions, but they did maintain 100% selectivity toward benzaldehyde. Although no tests were done to confirm if the doped materials were catalytic in nature, the doped materials showed percent conversion to benzaldehyde and excellent percent selectivity toward benzaldehyde. These results indicate that the material may have the potential to be a catalyst.

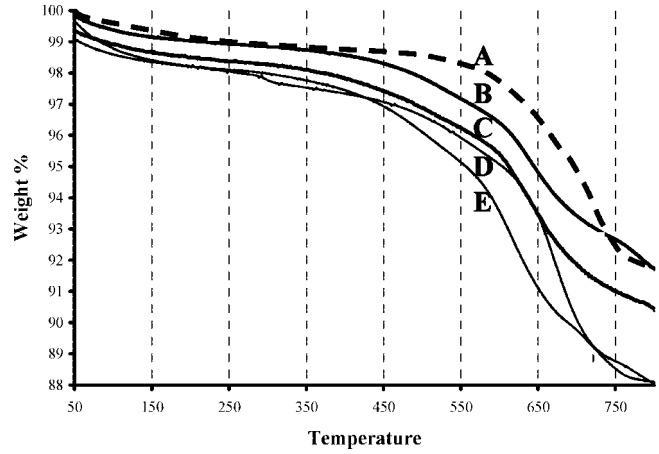

Figure 4. Thermogravimetric analysis profiles of doped K-OMS-2 samples. (A) K-OMS-2, (B) 1% W-ate, (C) 2% W-ate, (D) 1% WBr, and (E) 2% WBr.

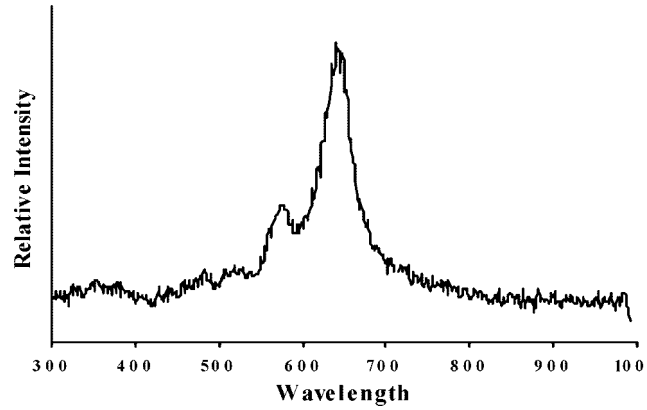

Figure 5. Raman spectra for a 1% tungsten-doped K-OMS-2 showing the F_{2g} peak at 580 cm^{-1} and the A_{1g} peak at 650 cm^{-1}.

Rietveld Refinement. Calculated and observed XRD patterns for the reference K-OMS-2 sample and the 1.33% W-ate sample are shown in Figures 6 and 7. Lattice parameters from refinements of the K-OMS-2 reference sample, 1.33% and 2% W-ate samples are listed in Table 2, and the structure of the 2% W-ate sample is shown in Figure 8.[33] There are no measurable differences in the lattice parameters (Table 2) or Mn coordinates (supplementary data) for K-OMS-2 doped with 1.33 and 2 mol% W and those of the reference K-OMS-2 sample. These results might have been expected, given the low concentration of W in the doped samples and the similar crystal radii of the candidate

(28) Julien, C. M.; Massot, M. *Mater. Sci. Eng., B* **2003**, *97*, 217.
(29) Julien, C. M.; Massot, M.; Poinsignon, C. *Spectrochim. Acta, Part A* **2004**, *60*, 689.
(30) Malinger, K. A.; Ding, Y. S.; Sithambaram, S.; Espinal, L.; Gomez, S.; Suib, S. L. *J. Catal.* **2006**, *239*, 290.
(31) Cazzanellia, E.; Vinegonib, C.; Mariottob; G.; Kuzminc, A.; Purans, J. *Solid State Ionics* **1999**, *123*, 67.
(32) Frost, R.; Duong, L.; Weier, M. *Spectrochim. Acta, Part A* **2004**, *60* (8−9), 1853.
(33) Downs, R. T.; Hall-Wallace, M. The American Mineralogist Crystal Structure Database. *Am. Mineral.* **2003**, *88*, 247−250 (XTALDRAW available from http://www.geo.arizona.edu/xtal/group/software.htm).

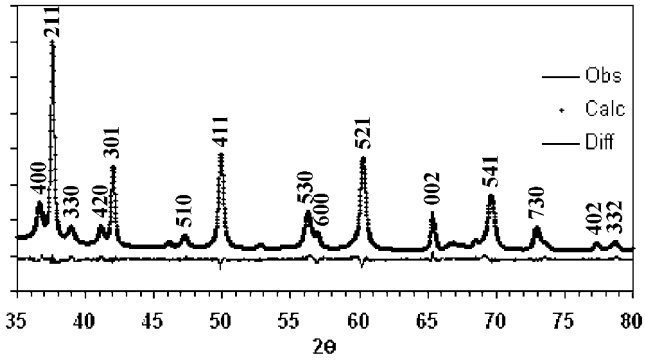

Figure 6. Powder X-ray diffraction patterns for refinement spectra of the reference K-OMS-2 pattern.

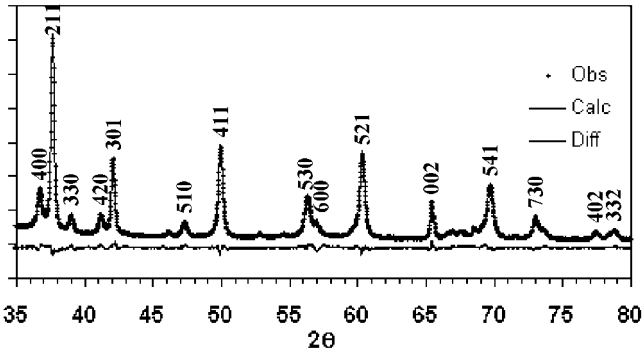

Figure 7. Powder X-ray diffraction patterns for refinement spectra of the 1.33% W-ate [W] K-OMS-2.

Table 2. Reitveld Refinement Data and Formula Calculated from a 2% W-ate Sample

	K-OMS-2	2% W-ate	1.33% W-ate
a (Å)	9.815	9.8163	9.8041
c (Å)	2.847	2.855	2.852
cell vol	274.3	275.1	274.1
params		18	18
	(JCPDS 29−1020)		
refinement formula		$K_{0.087}W_{0.023}Mn_{0.977}O_2$	

octahedrally coordinated cations $^{VI}W^{6+}$, $^{VI}W^{4+}$, $^{VI}Mn^{3+}$ HS, $^{VI}Mn^{3+}$ LS, and $^{VI}Mn^{4+}$.[2,3] Because the atomic scattering factor for W is a factor of 3 to 4 larger than that of Mn, it is expected that structure factors (F_{hkl}^2) for the doped materials would be measurably larger than those for reference K-OMS-2, but a consistent relationship is not observed. It was found, however, that attempts to refine the structures of the doped materials by including only Mn on the octahedral site produced fractional occupancies greater than one, indicating the presence of a heavier atom on that site.

Discussion

The Rietveld refinement confirms that the W atoms are located within the octahedral framework of K-OMS-2 and lattice parameters and atom coordinates show no measurable difference in lattice parameters between the doped samples and the reference material. The results showed that an occupancy of greater than one for the octahedral Mn sites was obtained when the assumption of only Mn in the octahedral Mn sites was refined. This result indicates the presence of atoms that are heavier than Mn atoms in these sites. Thus, the refinement confirms that the W atoms occupy the Mn sites in the structure. No extra atoms besides K^+ were detected in the tunnel sites.

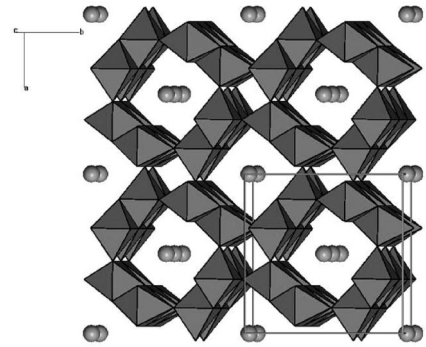

Figure 8. Structure for [W] K-OMS-2 showing the arrangement of octahedra looking slightly off center down the *c*-axis. The spheres are the K atoms and the box in the lower right corner is the unit cell. Structure drawn with XTALDRAW.[33]

Table 3. Ionization Potentials for Successive W[34] and Mn[35] Ions

		ionization potential (eV)		ionization potential (eV)
first	$W^0 \rightarrow W^+$	7.98	$Mn^0 \rightarrow Mn^+$	7.435
second	$W^+ \rightarrow W^{2+}$	16.1	$Mn^+ \rightarrow Mn^{2+}$	15.640
third	$W^{2+} \rightarrow W^{3+}$	25.2	$Mn^{2+} \rightarrow Mn^{3+}$	33.667
fourth	$W^{3+} \rightarrow W^{4+}$	37.4	$Mn^{3+} \rightarrow Mn^{4+}$	51.2
fifth	$W^{4+} \rightarrow W^{5+}$	50.6	$Mn^{4+} \rightarrow Mn^{5+}$	72.4
sixth	$W^{5+} \rightarrow W^{6+}$	64.8	$Mn^{5+} \rightarrow Mn^{6+}$	95
seventh	$W^{6+} \rightarrow W^{7+}$	119.7	$Mn^{6+} \rightarrow Mn^{7+}$	119.27
eighth			$Mn^{7+} \rightarrow Mn^{8+}$	196.5

The Rietveld refinements confirm that the [W] K-OMS-2 material is isostructural with tetragonal (*I*4/*m*) hollandite. The unit-cell parameters refined for two of the samples (Table 2) show a high correlation to the reference K-OMS-2 sample, reflecting that the difference in the amount of W in the material did not significantly affect the overall unit cell parameters.

The oxidation state of tungsten has not been elucidated, but there are several reasons to assume the oxidation state of W^{6+}. From periodic trends, the third row transition metals generally prefer their highest oxidation state. The tungsten ion in the starting solution is W^{6+}, and because of its lower ionization potential than Mn^{7+}, the Mn^{7+} would be reduced before the W^{6+} while refluxing (see Table 3). The oxidation state of W^{4+} is the same as Mn^{4+} and may not impart significant changes in average oxidation state of the material because of the similarity in oxidation states. W^{6+} would introduce a larger change in the oxidation state and could impart the more drastic changes that occurred in the chemical properties of the material.

Charge balance on substitution of hexavalent tungsten for three or four-valent manganese in the K-OMS-2 formula is maintained by coupled substitution with an octahedral vacancy ($^{VI}\square^{\circ}$).

(34) Koch-Bienemann, E.; Berg, L.; Czack, G.; Wagner, J. *Gmelin Handbook of Inorganic and Organometallic Chemistry−W Tungsten A2 Physical Properties (System-NR 54)*, 8th ed.; Springer-Verlag: Berlin, 1987; pp 85 and 93.

(35) Kugler, H. K. *Gmelin Handbook of Inorganic and Organometallic Chemistry−Manganese The Element (System-NR 56)*; 8th ed.; Springer-Verlag: Berlin, 1973; p 195.

Substitution of $^{VI}W^{6+}$ for $^{VI}Mn^{4+}$ in K-OMS-2,

$$2\,^{VI}W^{6+} + {}^{VI}\square^{\circ} \leftrightarrow 3\,^{VI}Mn^{4+} \quad (4)$$

is described by the formula

$$K_X W^{6+}{}_{2Y}\square^{\circ}{}_{Y}Mn^{4+}{}_{1-X-3Y}Mn^{3+}{}_{X}O_2 \quad (5)$$

The upper limit of W concentration all $^{VI}Mn^{4+}$ is replaced by $^{VI}W^{6+}$ ($3Y = 1-X$), but this concentration of $^{VI}\square^{\circ}$ will probably lead to structural collapse well before that limit is reached.

Substitution of $^{VI}W^{6+}$ for $^{VI}Mn^{3+}$ is also coupled with an octahedral vacancy to balance charge,

$$^{VI}W^{6+} + {}^{VI}\square^{\circ} \leftrightarrow 2\,^{VI}Mn^{3+} \quad (6)$$

Because charge balance is achieved by replacement of $^{VI}Mn^{3+}$, the concentration of which is balanced by $^{VIII}K^{1+}$ in the undoped structure,[13] insertion of the $^{VI}W^{6+} + {}^{VI}\square^{\circ}$ pair is necessarily coupled with the redox exchange, leading to the formula

$$K_X W^{6+}{}_{Y}\square^{\circ}{}_{Y}Mn^{4+}{}_{1-X}Mn^{3+}{}_{X-2Y}O_2 \quad (7)$$

As shown in Table 1, analyzed [W] K-OMS-2 fits this formula. The maximum content of $^{VIII}K^{1+}$ ($X = 0.125$) in the tunnel site limits ^{VI}W concentration to $n_W = 1/2 n_K \leq 0.0625$, a result consistent with failure of syntheses with 4% or more W, as indicated by the diffraction data.

The Raman spectrum of the doped K-OMS-2 material has the same spectrum as previously reported undoped K-OMS-2 material. This indicates that the doped and undoped material contain similar manganese oxide species. Tungsten present in the framework may not have been detected due to detection limits. The lack of additional peaks suggests that there were no detectable free tungsten oxides present. Tungsten oxides have Raman active modes, so if present in significant amounts, they would have been detected.

The TGA data show similar profiles to K-OMS-2, but there was about a 100 °C decrease in the initial oxygen loss; therefore, the refractory nature of tungsten did not help the thermal stability of the substituted materials. The lower thermal stability exhibited in the TGA profiles was possibly caused through instabilities created by vacancies due to the tungsten substitution, ionic radius mismatches, and electrical changes.

The insertion of tungsten into the material led to changes in the chemical properties of the substituted material. These changes were likely caused by the restricted electron flow from inserting a more positively charged species into the material as measured by the increase in the resistivity of the material by at least several orders of magnitude. Such insertion can cause the tungsten dopant to act as a trap for preventing electron transfer. The oxidation reaction chosen was an oxidation reaction that utilizes the mobile lattice oxygen ions of K-OMS-2. Because the electrons were more localized, they did not transfer to the oxygen atoms and then form the active oxygen species thus inhibiting the oxidative power of the doped material. These unique aspects of tungsten doped K-OMS-2 could be used to fine-tune the catalytic properties for different reactions that require a porous material with tunable oxygen mobility.

Conclusion

The refinements of the synthesized [W] K-OMS-2 material confirm that the W atoms occupy the Mn sites in the structure, and that the synthesized [W] K-OMS-2 material was isostructural with tetragonal ($I\,4/m$) hollandite for doping ratios of 2% and below. The oxidation state of tungsten was assumed to be W^{6+} due to periodic trends, ionization potential, and changes in the chemical properties of the doped material. From the data gathered, the analyzed [W] K-OMS-2 fit a formula of $K_X W^{6+}{}_{Y}\square^{o}{}_{Y}Mn^{4+}{}_{1-X}Mn^{3+}{}_{X-2Y}O_2$. The inability to synthesize a 4% or greater doped material is due to the maximum content of $^{VIII}K^{1+}$ (X=0.125) in the tunnel site limiting the ^{VI}W concentration to $n_W = 1/2\ n_K \leq 0.0625$. Resistivity of the material increased by over an order of magnitude upon doping, whereas the thermal stability and catalytic activities of the material varied relative to the amount of dopant used in the reaction mixture.

Controlling the properties of doped K-OMS-2 by using different amounts of dopant along with different dopants could lead to the ability to fine-tune the properties of the material to the designated task, such as different catalysis reactions. Doping K-OMS-2 with two different metal ions simultaneously could allow more routes to adjusting properties of the material. High valance tungsten dopants act as efficient traps for quenching electron transfer in these systems producing materials with excellent resistivity. With the ability to adjust the conductivity, these materials could lead to various applications including new battery materials and novel sensors. Such marked changes in conductivity have not been observed on doping K-OMS-2 materials with other cations.

Acknowledgment. The authors thank the Chemical Sciences, Geosciences and Biosciences Division of the Office of Basic Energy Sciences, Office of Science, U.S. Department of Energy, for support of this work.

Supporting Information Available: Crystallographic files for the 2% and 1.33% refined material (CIF). This material is available free of charge via the Internet at http: //pubs.acs.org.

CM801146M